ACS NANO

Subscriber access provided by Univ.bibliothek Bayreuth

Articles

Specific Features of Defect Structure and Dynamics in the Cylinder Phase of Block Copolymers

Andriana Horvat, G. J. Agur Sevink, Andrei V. Zvelindovsky, Alexei Krekhov, and Larisa Tsarkova

ACS Nano, **2008**, 2 (6), 1143-1152• DOI: 10.1021/nn800181m • Publication Date (Web): 07 June 2008

Downloaded from http://pubs.acs.org on May 14, 2009

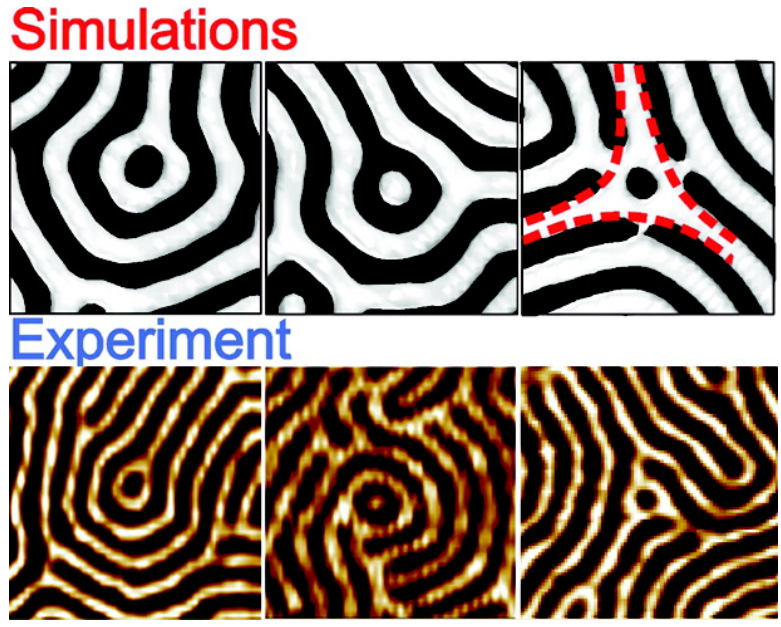

More About This Article

Additional resources and features associated with this article are available within the HTML version:

- Supporting Information
- Links to the 1 articles that cite this article, as of the time of this article download
- Access to high resolution figures
- Links to articles and content related to this article
- Copyright permission to reproduce figures and/or text from this article

View the Full Text HTML

ACS Publications
High quality. High impact.

ACS Nano is published by the American Chemical Society. 1155 Sixteenth Street N.W., Washington, DC 20036

Specific Features of Defect Structure and Dynamics in the Cylinder Phase of Block Copolymers

Andriana Horvat,[†] G. J. Agur Sevink,[‡] Andrei V. Zvelindovsky,[§] Alexei Krekhov,[⊥] and Larisa Tsarkova[†,*]

[†]Physikalische Chemie II, Universität Bayreuth, D-95440 Bayreuth, Germany, [‡]Leiden Institute of Chemistry, Leiden University, PO Box 9502, 2300 RA Leiden, The Netherlands, [§]Department of Physics, Astronomy and Mathematics, University of Central Lancashire, Preston, PR1 2HE, United Kingdom, and [⊥]Theoretische Physik I, Universität Bayreuth, D-95440 Bayreuth, Germany

ABSTRACT We present a systematic study of defects in thin films of cylinder-forming block copolymers upon long-term thermal or solvent annealing. In particular, we consider in detail the peculiarities of both classical and specific topological defects, and conclude that there is a strong "defect structure—chain mobility" relationship in block copolymers. In the systems studied, representative defect configurations provide connectivity of the minority phase in the form of dislocations with a closed cylinder end or classical disclinations with incorporated alternative, nonbulk structures with planar symmetry. In solvent-annealed films with enhanced chain mobility, the neck defects (bridges between parallel cylinders) were observed. This type of nonsingular defect has not been identified in block copolymer systems before. We argue that topological arguments and 2D defect representation, sufficient for lamellar systems, are not sufficient to determine the stability and mobility of defects in the cylindrical phase. *In-situ* scanning force microscopy measurements are compared with the simulations based on the dynamic self-consistent mean field theory. The close match between experimental measurements and simulation results suggests that the lateral defect motion is diffusion-driven. In addition, 3D simulations demonstrated that the bottom (wetting) layer is only weakly involved into the structure ordering at the free surface. Finally, the morphological evolution is considered with the focus on the motion and interaction of the representative defect configurations.

KEYWORDS: block copolymers · thin films · defect structure and dynamics · nanostructured soft matter

Thin films of block copolymers have been intensively studied over the last decades to gain understanding and control of the parameters affecting the microdomains structure, orientation, and order.[1–3] Surface fields are important external potentials which influence the equilibrium structures and the dynamics of microdomains. Substrate modification by chemical or topographic patterning is now widely used to control the selectivity and the strength of the polymer-substrate interactions and thus to guide the morphology and its orientation as well as long-range order in nano-patterned films.[4–7]

It is recognized that topological defects in the local microdomain structure decrease the long range periodicity and limit the technological performance of block copolymer materials. The generation and annihilation of topological defects are the elementary processes by which long range order evolves in microdomains under the influence of thermal energy[8,9] and application of external fields.[10,11] Therefore, defect analysis is important for establishing the transport mechanisms in nanostructured soft materials.

Several theoretical approaches have been developed to describe 2D defect configurations,[12,13] their interfacial properties,[14,15] and their role in microdomain reorientation.[16] In experiments, detailed information about structure and dynamics of individual defects in block copolymers is accessed by non-destructive time-resolved real-space imaging techniques, such as scanning force microscopy (SFM). The seminal work by Harrison *et al.* on defect evolution in stripped surface pattern[17] and related studies,[5,18–20] convincingly demonstrated that classical defects such as disclinations and dislocations, widely known from the solid crystals and nematic liquid crystal phases, play an important role in the ordering dynamics of block copolymers microdomains. The observations of defects in sphere-forming diblock copolymer films allowed conclusions to be drawn regarding the mechanisms of 2D crystal to hexatic transition, and on further melting *via* continuous defect generation process.[21,22] Also, grain coarsening in hexagonally ordered dotlike structures which are composed of either of spheres[23,24] or standing cylinders[25] has been analyzed in detail.

The research mentioned above focused on the similarities of defect interaction and their motion in block copolymers and thermotropic nematics or smectics. Thermo-

*Address correspondence to larisa.tsarkova@uni-bayreuth.de.

Received for review December 19, 2007 and accepted May 14, 2008.

Published online June 7, 2008.
10.1021/nn800181m CCC: $40.75

© 2008 American Chemical Society

tropic liquid crystals, however, are one-component homogeneous systems and are characterized by a nonconserved orientational order parameter. In contrast, in block copolymers the local concentration difference between two components is essentially conserved. In this respect, the microphase separated structures in block copolymers are anticipated to have close similarities with lyotropic systems which are composed from polar medium (water) and nonpolar medium (surfactant structure). The phases of the lyotropic systems (such as lamella, cylinder or micellar phases) are determined by the surfactant concentration. Similar to lyotropic phases, the morphology in block copolymers is ascertained by the volume fraction of the components and their interaction. Therefore, in lyotropic systems and in block copolymers the dynamics and annihilation of structural defects require a change in the local concentration difference between components as well as a change in the orientational order. Consequently, if single defect transformations could be monitored in real time and space, block copolymers could be considered as suitable model systems for studying transport mechanisms and phase transitions in two-dimensional fluid materials such as membranes,[26,27] lyotropic liquid crystals,[28] and microemulsions.[29]

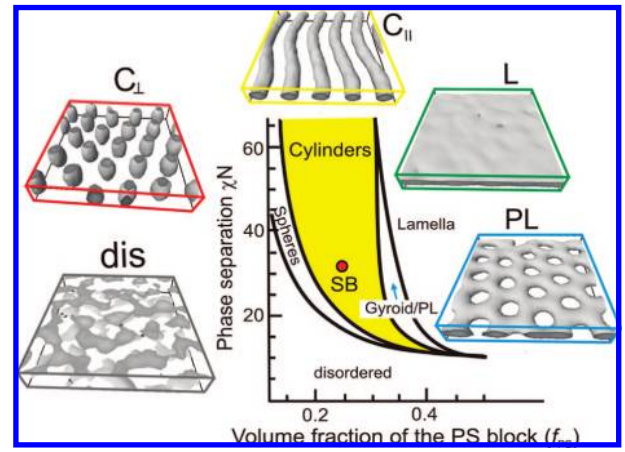

Figure 1. Schematically represented phase diagram of AB diblock copolymer melt.[30] "SB"-Labeled point indicates the parameters of the SB block copolymer under the experimental conditions reported in this study. The DSCFT simulations illustrate surface structures that are predicted theoretically and observed experimentally in thin films of cylinder-forming block copolymers under surface fields or thickness constraints: disordered phase (dis), vertically oriented cylinders ($C_{\perp}$), cylinders aligned parallel to the film plane ($C_{\parallel}$), lamella (L), and hexagonally perforated lamella (PL) phases.

In this work, we observe structural defects and their short- to long-term dynamics in block copolymer films using SFM, including *in-situ* measurements at elevated temperatures with high temporal resolution, and we compare the experimental findings to simulations based on the dynamic self-consistent mean field theory (DSCFT). In the experiments we used polystyrene-*block*-polybutadiene copolymer, designated here as SB and composed from the polystyrene (PS) and polybutadiene (PB) blocks. In simulations, the molecular model is an A3B12A3 Gaussian chain with A and B corresponding to the PS and to the PB components, respectively. We focus on specific defects in the cylinder phase which are kinetically trapped in thermal equilibrium during the lateral ordering of lying microdomains. The strength of our approach is that 2D structures and defects visualized with SFM are directly compared with computational simulations which give access to the "bulk" structure in the interior of the film. We distinguish between classical, modified, specific, and grain boundary defect configurations. For each defect type, we address its relative stability, interaction with the other defect types, and its role in the overall structure development.

With this approach, we discovered the strong correlation between defect structure and chain mobility, a feature which is specific to block copolymer materials due to the covalent bonding between the blocks and their large molecular weight and a feature which is not common in nematic thermotropic and lyotropic liquid crystals. The interconnectivity of the polymer chains is then manifested in the lateral propagation of a complex 3T-junction-defect, which has been captured both by *in-situ* SFM measurements and by DSCFT simulations. Finally, we discuss the lateral migration of complex and specific structural defects which are involved in the coarsening of surface patterns.

RESULTS AND DISCUSSION

Phase Behavior in Thin Films. As indicated in Figure 1 the bulk structure of SB diblock copolymer resides well in the cylinder regime within the mean-field-calculated phase diagram.[30] However, it is well established that confinement and surface fields effects in thin films of cylinder-forming block copolymers can cause the microdomains to deviate from the corresponding structure in bulk.[31] Simulated images in Figure 1 are examples of surface structures[32] which are also identified experimentally in thin films of cylinder-forming di- and triblock copolymers. In particular, the nonbulk perforated lamella (PL) and lamella (L) phases were reported for this type of block copolymers under strong surface fields or thickness constraints.[30,31,33,34] The PL structure can be viewed as alternative layers of block copolymer components with hexagonally ordered perforations in the minority phase and is tentatively similar to mesh-like liquid crystalline phase. Since to the best of our knowledge the gyroid phase has not yet been reported for thin films of diblock copolymers and of two-component triblock copolymers, the PL phase in the above systems presumably represents a 2D analogue of the bicontinuous gyroid structure.

Classification of Characteristic Defects. ***Classical Defects.*** The theory and classification of defects are well-developed

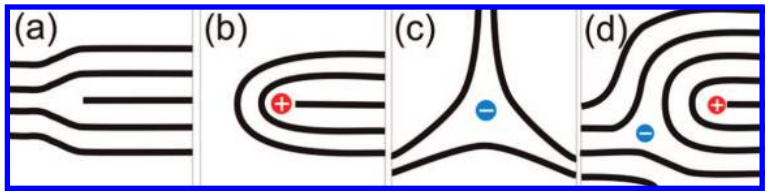

Figure 2. Schematic representation of classical topological defect configurations: (a) edge dislocation; (b) +1/2 disclination; (c) −1/2 disclination; and (d) paired ±1/2 disclinations.

for certain types of materials such as solid crystals, nematic liquid crystals, and superfluids.[35,36] In general, a topological defect is characterized by a core region (point, line, or wall) where the order parameter is destroyed and a far field region where it relaxes slowly in space. The most common topological defects in block copolymers are generally analogous to that in liquid crystals, so the nomenclature classifying them is similar.[35]

Figure 2 displays sketches of classical topological defects which are common to different types of materials including block copolymers: an edge dislocation (a), +1/2 disclination (b), -1/2 disclination (c) and a pair of oppositely charged disclinations (d). Such defects have been considered in the earlier studies on microdomain ordering in cylinder- and lamella-forming block copolymers.[17–19]

Figure 3 presents examples of simulated (top panel) and measured classical defects in triblock and diblock copolymers, respectively. In these pictures as well as in the following SFM and simulated 2D images, the white color corresponds to PS cylinders (minority phase). In a two-component system, topological defects can be formed by each phase. Images a,e and b,f in Figure 3 display edge dislocations which are formed by white and dark compartments, respectively. These defect configurations are topologically identical. Similarly, shown in Figure 3c,g, +1/2 disclination can be transformed into +1/2 disclination in Figure 3d,h by color inversion. Purely topological arguments are sufficient to describe defects in films with upstanding lamella; here a topological defect always implies the abruption of one component. In contrast, in cylinder phase the majority dark-colored matrix (PB phase) is always interconnected, while the 2D representation of topological defects conceals this important property.

To account for the real 3D structure of cylindrical microdomains, we denote the configurations in Figure 2a,e and c,g as cylinder-phase defects (cyl-dislocation and +1/2 cyl-disclination), and the configurations in Figure 2b,f and d,h as matrix defects (m-dislocation and m-disclination). In our systems, cyl-dislocations (Figure 2a,e) generally develop during the early stages of film annealing when the overall defect density is high. In well-equilibrated films, cyl-dislocations are less frequent as compared to m-dislocations (Figure 2b,f), a finding that is in agreement with the earlier studies.[19,20] The reduced stability of cyl-dislocation is likely caused by the higher energy costs of an open-cylinder-end defect.

The lifetime of these defects depends on their surrounding. Edge dislocations are highly mobile defects when they interact with an oppositely charged pair, or with disclinations. Isolated dislocations, for example, in the middle of a large cylinder grain, are harder to annihilate. Their relative immobility is attributed to the high energy costs to restructure the ordered surrounding. The same energetic arguments account for the trapping of +1/2 disclinations of both types (Figure 3c,d) in well-ordered samples.

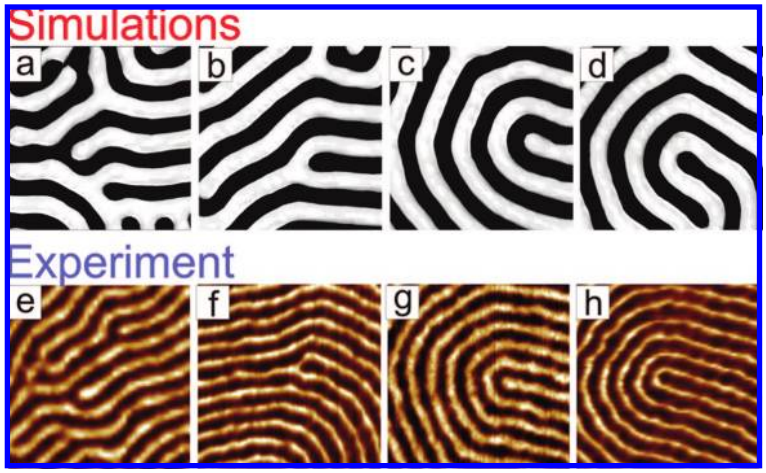

Figure 3. Simulated images (top panel) and SFM phase images (300 nm × 300 nm) presenting classical topological defect configurations in lying cylinders: (a,e) cyl-dislocation; (b,f) m-dislocation (see definition in text); (c,d) +1/2 cyl-disclination and (g,h) +1/2 m-disclination. SB films have been annealed under 70% of the saturated vapor pressure of chloroform. Here and in the following simulated/experimental images white stripes correspond to the A minority phase/PS cylinders; dark stripes correspond to B majority phase/PB matrix.

The motion of cyl- or m-dislocations perpendicular to the cylinder axis involves the consecutive opening and relinking of a cylinder connection. These elementary steps of dislocation dynamics have been recently accessed with *in-situ* SFM imaging.[37] The estimated typical time for the rejoining of a dislocation was ~10 s. The related activation energy ~30 J/mol is several orders of magnitude lower compared to the value obtained by SFM snap-shot experiments.[19] Importantly, m-dislocations (Figure 3b,f) can propagate along the cylinder axis without diffusion across the PS−PB interface.[37]

Modified Classical Defects. The rich phase behavior of cylinder-forming block copolymers is re-

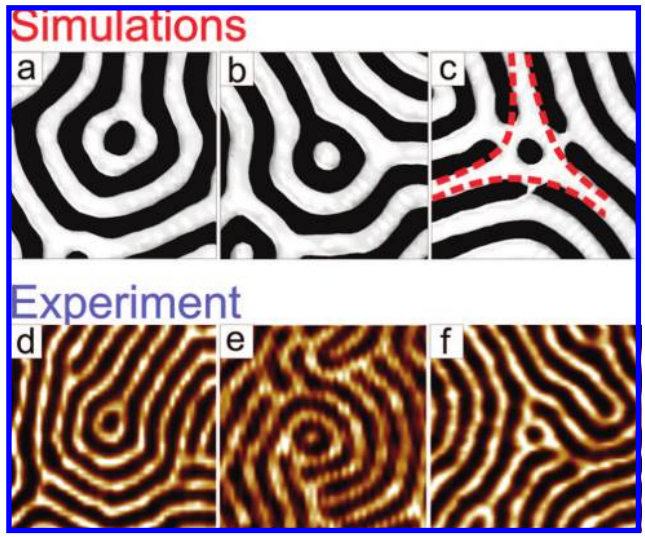

Figure 4. Simulated images (top panel) and SFM phase images (300 nm × 300 nm) presenting specific defect configurations: +1/2 disclination (a,d) and −1/2 disclination (c,f) with incorporated PL fragment; (b,e) +1/2 dot-disclination. SB films have been annealed under 50% of the saturated vapor pressure of chloroform.

flected in the modification of classical defects by incorporation of elements of nonbulk structures. Defects in Figure 4a,d are tentatively attributed to +1/2 disclination with an incorporated PL ring. In this kind of defect, the PL cell often has a distorted shape and somewhat large dimensions compared to a hexagonally ordered PL unit site. It is typically isolated from other PL-like defect sites and appears to be position-trapped. The defect in Figure 4b,e can be obtained by phase inversion in the previously described +1/2 disclination and is therefore topologically equivalent to the above defect. However, the white dot in the middle (Figure 4b,e) can be attributed to vertically oriented cylinders, spheres, or cylinders with upstanding necks. Such defects are typically formed at early stages of structure equilibration; they stick to their original position and annihilate rather slowly due to missing lateral connectivity in the minority phase.

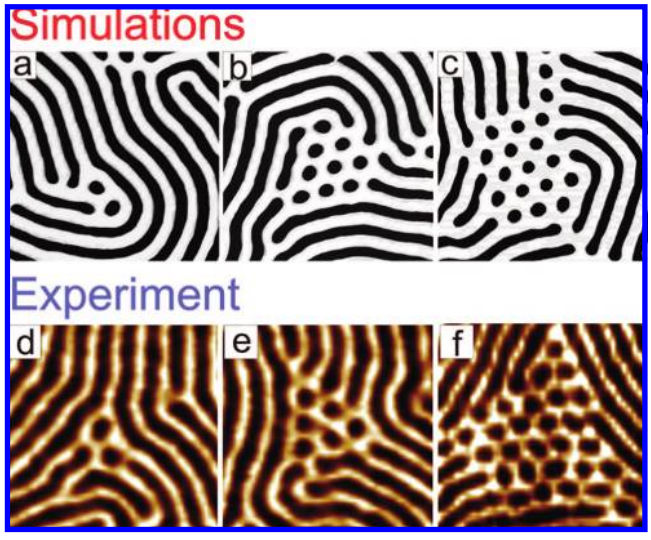

Figure 5. Simulated images (top panel) and SFM phase images (300 nm × 300 nm) depicting specific configurations of −1/2 disclinations with different PL-cluster size. SB films have been annealed under 50% of the saturated vapor pressure of chloroform.

Figure 4c,f displays another example of a representative specific defect. This configuration is identified as a modified classical −1/2 disclinations with incorporated PL structure. Such defects are typically paired with +1/2 disclinations and are trapped at *three*-cylinder-grain junctions. The PL structure lacks the axial symmetry; therefore it effectively compensates large disorientations of cylinder grains. Additionally, the appearance of the nonbulk PL phase as a defect component in the cylinder phase can be justified by low interfacial tension between these phases.[38] Since the dimensions of the hexagonally ordered PL and cylinder phases are compatible, the excess of the chain stretching/confinements at defect cylinder sites is released by the local phase transition.

The modified −1/2 disclination can contain PL clusters of varied size (Figure 5). Generally, the size and the lifetime of the PL-defects depend on the particular experimental conditions. On one hand, they can be considered as a metastable transient phase which enhances the connectivity of the minority component as compared to the cylinder phase, and therefore facilitates the annihilation of defects. The lifetime of such temporal phases with a cluster size of ~1−10 PL rings ranges from minutes to hours.[39] On the other hand, these ring-like PL-defects may appear as nuclei of a stable PL grain when a small thickness gradient promotes coexistence of PL/$C_{\parallel}$ phases (Figures 5c,f and 11).[32,34]

Another example of a frequently observed position-trapped configuration denoted as the horseshoe defect is presented in Figure 6. This defect can be viewed as a core region of +1/2 disclination next to a PL cluster. It is as well observed in DSCFT simulations which in some instances reveal the connection of this defect to the bottom layer of microdomains (Figure 6c). The annihilation of such defects through the formation of a transient nonbulk lamella phase was captured by *in-situ* SFM (Figure 6d).[37] The horseshoe defect is highly incompatible with ordered in-plane structures, and the local transition to lamella phase provides higher in-plane chain mobility as compared to that in the cylinder phase.

Specific Defects. Figure 7 presents a specific neck defect which, to our knowledge, has never been identified before in block copolymer films. This bridge-like connection between neighboring parallel cylinders can be viewed as a closely interacting pair of m-dislocations (Figure 7a and related sketch). Such necks provide connectivity of the minority phase and thereby facilitate material transport without crossing the PS−PB interface. Since the annihilation of a neck-defect does not require a discontinuous change of the order parameter, it is not a singular defect. Necks are frequently observed

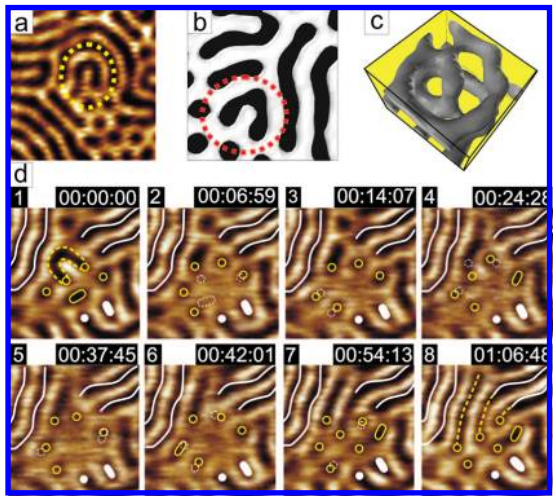

Figure 6. SFM phase image (a) (300 nm × 300 nm) and simulated images (b,c) presenting the "horseshoe" defect. (d) Selected SFM phase images (250 nm × 250 nm) from the consecutively saved sequence illustrating the annihilation of a "horseshoe" defect (marked by dashed lines in frame 1). Solid white lines and filled symbols mark lattice sites which remain unchanged during the transformation. Empty symbols indicate lattice sites at the boundary of the transient lamella phase. The previous position of moving lattice sites is shown by dashed symbols. In frame 8, thick dashed lines mark cylinder domains which replace the "horseshoe" defect (frame 1). *In-situ* SFM imaging has been done at 105 °C.

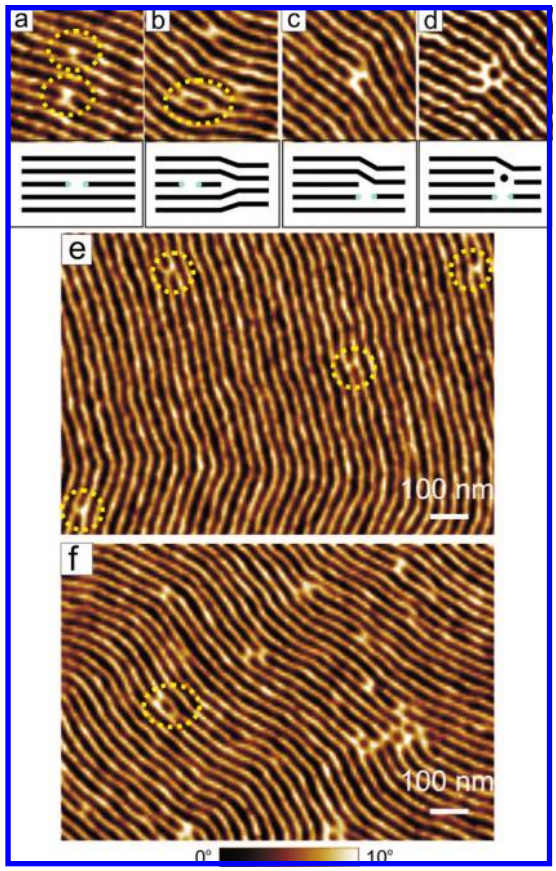

Figure 7. SFM phase images of surface structures in SB films, which were equilibrated under 70% of the chloroform-saturated atmosphere, showing specific neck defects (a,e) (highlighted by white (yellow) circles); interaction of neck-defects with m-dislocations (b,c), and with a single PL ring (d). Image f indicates the elementary steps of the lateral defect motion and interaction.

in the ordered cylinder phase under conditions which provide sufficient chain mobility (for example, in swollen SB films with the polymer volume fraction below ~0.8, Figure 7e,f). Such necks can group with m-dislocations along or across the cylinder axis (Figure 7 panels b and c, respectively) or with PL rings (Figure 7d). Interestingly, in DSCFT simulations neck defects are not seen in the ordered cylinder phase. This fact likely indicates a small energy difference between the neck defect and the defect-free cylinders. Considering the experimental conditions when the necks between cylinders form, we conclude that their origin is driven by local concentration fluctuations.

The observed SB films neck defects are similar to those found in liotropic liquid crystals. In particular, the important transport functions of the bridging connections in lyotropic lamella phase have been recently reported.[28] In this study, the abrupt increase of the diffusion coefficient across the lamella upon approaching the lamella-isotropic phase transition has been interpreted in terms of neck defects connecting the surfactant structure. Additionally, the formation of nonsingular neck defects is tentatively similar to the initial stages of the membranes/vesicles fusion.[26] Note that in thermotropic liquid crystals such defects are prohibited due to a nonconserved nature of the order parameter.

Grain Boundary Defects. Figure 8 presents examples of extended grain boundary defects. The T-junction defect (Figure 8a,d) is one of the most stable defect configurations and forms at large angles of disorientation (~80−90°) between two cylinder or lamella[40] grains. In the cylinder phase, T-junctions compensate for strong disorientation of grains and at the same time provide connectivity of PS cylinders (white stripes) between neighboring grains while the majority PB matrix (dark stripes) remains interconnected. We note that the connectivity function of a T-junction in most cases can not be realized in the lamella phase as it always abruptly terminates one component (mostly, the minority component[40]). In the following, we describe the lateral mobility of such complex T-junction defects.

The extended defect in Figure 8b,e is represented by a chain of PL cells along the grain boundary and can be considered as a modified T-junction defect. Such configuration indicates the tendency of the system to undergo the cylinder-to-PL phase transition. The

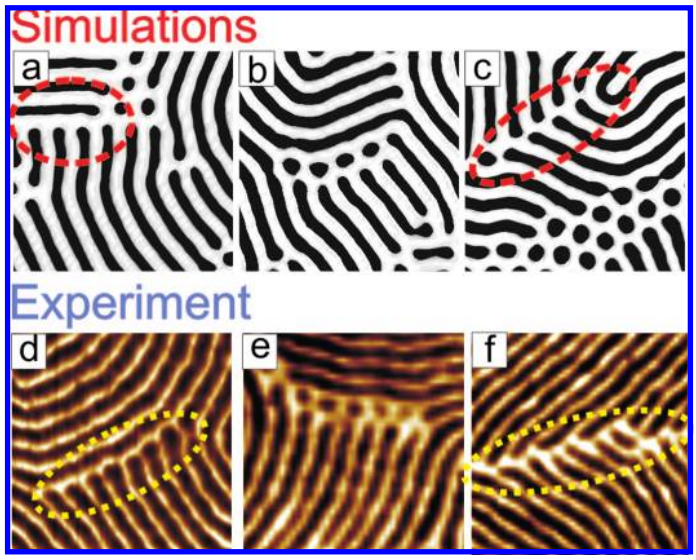

Figure 8. Simulated images (top panel) and SFM phase images (300 nm × 300 nm) presenting grain boundaries defects: (a,d) extended T-junctions configuration; (b,e) chain of PL rings at grain boundary; (c,f) grain boundary defect between cylinder grains with a disorientation angle of ~75°. SB films have been annealed under 70% (d,f) and 55% (e) of the saturated vapor pressure of chloroform.

boundary defect in Figure 8c,f presents the case where two cylinder grains meet at a disorientation angle of 70−75°. This grain boundary is characterized by considerable distortion of microdomain dimensions in the junction sites; at the same time, the connectivity of the minority PS phase between the neighboring grains is preserved. However, we note that in most cases grain boundaries with such disorientation angles are marked by a narrow region with high density of classic and specific defects described above.

Dynamics of Complex Defects. ***Experiment.*** With *in-situ* SFM we followed the lateral movement of a 3T-junction defect which consists of four parallel cylinders connected to an orthogonally-oriented cylinder (Figure 9a). The SFM movie can be found as Supporting Information.[41] Selected frames from this movie and the respective sketches below each image (Figure 9a) present the characteristic steps of the defect propagation. As a guide for the eye, white (yellow) dots mark the open cylinder end. The position of this +1/2 disclination remains stable during imaging. Another characteristic reference point is a white-dot defect which is indicated by the arrow in frame 32 of Figure 9a. In Frame 32, the 3T-junction is positioned next to the marked +1/2 disclination (configuration A). About 9 minutes later, the 3T-junction appears to be separated by one cylinder from the disclination (frame 46 and configuration B). Finally, in frame 77 it is separated by two cylinders from the indicated disclination, still preserving its complex structure.

The details of these transformations are captured in the SFM-movie which covers more than 70 minutes of the continuous imaging. Since we have done the measurements with high temporal resolution, we plotted in Figure 9b a temporal pathway of this defect. Here the temporal and excited defect configurations are sorted along the vertical axis according to the number of cylinder open ends. Each type of symbol indicates the presence of a certain defect configuration such as the A, B, or C type as in Figure 9a, such as the intermediate 4T-junction configuration in frame 41 (inset in Figure 9b), or a quite stable +1/2 disclination as in frame 56 (Figure 9b). When a configuration does not contain an open cylinder end (such as in frames 56 and 93 in Figure 9b) or a shape undulation (as the sock-like undulation in frame 31 of Figure 9b), then the symbols are placed on the horizontal dashed line. Any open cylinder end is configured as higher energy defect structure and the respective data-point is shifted up along the y-axis.

Figure 9b indicates that each of the configurations A, B, and C has a different lifetime. Configuration A was present for about 40 minutes with a short-lived break-up of the cylinder connections and shape undulations (excited configurations). The transition to configuration B was achieved *via* an intermediate 4T-junction defect. Configuration B was relatively short-lived, and changed quickly into a long-lived defect with +1/2 disclination (frame 56 in Figure 9b). The final step to configuration C proceeded with the consumption of the PL ring from the modified −1/2 disclination (as in Figure 4f). Configuration C appeared to be quite stable with almost no fluctuations. Importantly, in configuration C the 3T-junction now appears closer to the small PL patch (a nonbulk transient phase). Thus on a mesoscale level, the captured motion can be viewed as an elementary step towards the lateral separation of coexisting morphologies (see Figure 11).

During the captured lateral transformations, the complex 3T-junction defect has moved on a distance of two microdomain spacings ($a \approx 70$ nm) in $t \approx 70$ minutes. A simple estimation using the Einstein relation $a = (Dt)^{1/2}$ gives a diffusion constant of $D \approx 10^{-16}$ cm^2/s. This result indicates that the lateral diffusion of a complex stable defect configuration is 3−4 orders of magnitude smaller compared to the self-diffusion constant determined earlier for this system.[37]

Simulations. A lateral migration of the similar 3T-junction defect was followed with DSCFT simulations and is presented in Figure 10. Like in Figure 9b, defects are sorted along the *Y*-axis according to the number of cylinder open ends. Selected frames from the simulation movie[42] display characteristic (A and B) and intermediate stages of the 3T-junction movement. In simulations, the defect moved on one cylinder spacing to the right relative to the initial position A. Similar to the experimental observations, the movement of the complex 3T-junction defect proceeds *via* long-living intermediate structures with +1/2 disclination (marked by yellow (gray) squares in Figures 9b and 10). Moreover, the movement of the defect is directed towards the de-

veloping PL phase (right image in Figure 10). From the good agreement between the simulations and the experimental observations we conclude that DSCFT on a long time scale correctly describes defect dynamics in block copolymer films. From the above results, a single simulation step can be identified with a real experimental time of ~1−2 s. This value is in a good agreement with the earlier experimental and theoretical studies which are based on the comparison of the morphological phase transitions[38,43] rather than on the analysis of the lateral defect motion.

Another important conclusion which we have derived from the dynamic simulations of a film with a wetting layer is only the weak involvement of this bottom layer in the ordering of the structures at the free surface. Slight perturbations in the volume density at the wetting layer are seen exclusively below excited defect configurations such as open-cylinder-ends (see 3D simulation movie[42]).

Lateral Separation of Morphologies under Coexistence Conditions. Earlier theoretical and experimental studies have pointed to a relationship between the microdomain structures and transport mechanisms in block copolymer films. In particular, it is known that topological defects with open cylinder ends (such as vertically oriented cylinders, cylinders with necks, open-end dislocations) are indicative of the material transport perpendicular to the surface.[19,43,44] Such open-end structures appear during the early stages of terrace formation,[43] during the directional orientation of cylinders perpendicular to the surface by external fields,[22,45,46] and in thermal equilibrium at incompatible film thickness.[31] Here we focus on the specific defects which are associated with the lateral ordering of lying cylinder microdomains.

In the earlier studies on the phase behavior in SB films, we established conditions in which the cylinder phase is in thermal equilibrium with the PL structures.[34,47] At particular surface fields and segregation power, the slight thickness variation within the first layer of cylinders is reflected in the coexistence of two morphologies. Further, we noticed that the degree of the lateral separation of cylinder and PL phases essentially depends on the annealing conditions. Figure 11 presents SFM phase images of the surface structures in ~11/2-layer thick SB films which have been annealed (a) in vacuum at elevated temperature and (b) in the atmosphere of the chloroform vapor. Both images reveal coexistence of morphologies, however with drastically differing degree of the lateral separation (different grain sizes).

Figure 11a displays coexisting PL and cylinder grains of small sizes with a high defect density in the cylinder phase. In contrast, after solvent annealing the two morphologies are well separated and exhibit a high degree of long-range order. Since in both systems the χN parameter is estimated to be ~35 and thus the segregation power is assumed to be similar, the difference in the degree of the structure equilibration can be attributed to the chain mobility under given annealing conditions. Obviously, the efficiency of the microdomain

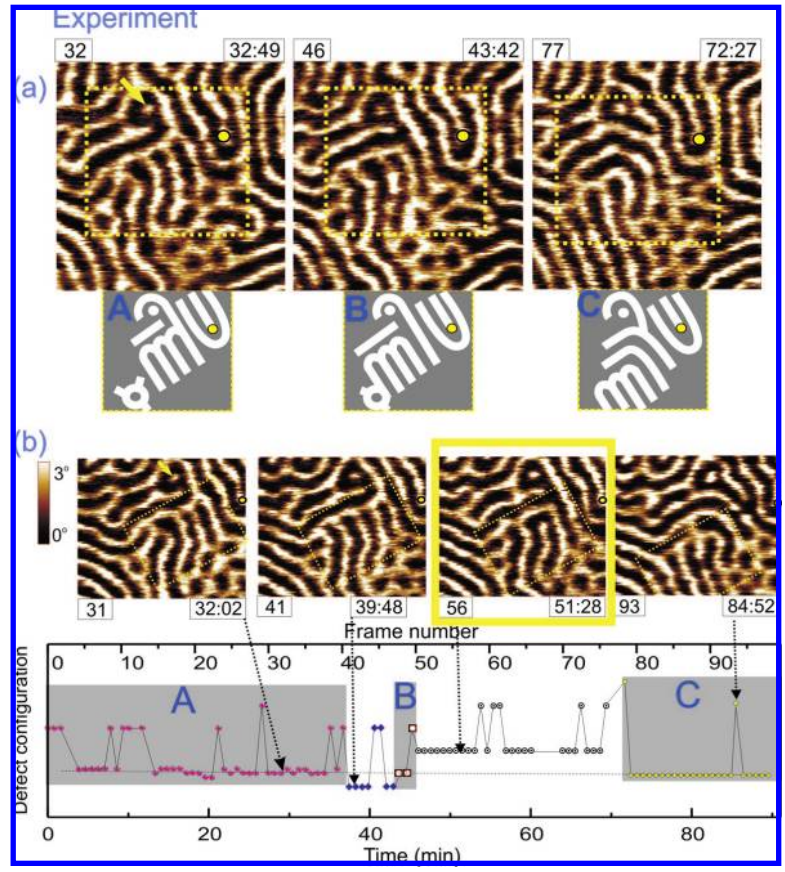

Figure 9. Dynamics of the 3T-junction defect. (a) SFM phase images from *in-situ* SFM movie (image size, 350 nm × 350 nm; the phase scale, 3°). Frame numbers and elapsed time of the SFM movie are indicated next to each frame. Configurations A, B, and C highlight the stages of the movement of the T-junction defect (marked with a white (yellow) square) relative to the indicated position-trapped defects. (b) Plot shows the evolution of temporal/excited configurations, which are sorted and grouped along the configuration coordinate according to the number of "open ends". SFM images (250 nm × 200 nm) in the upper panel are selected frames from SFM movie and present intermediate defect configurations.

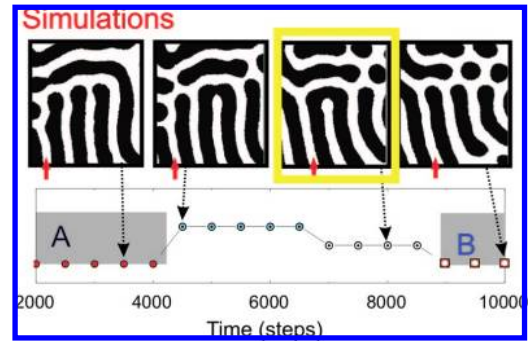

Figure 10. Temporal evolution of the 3T-junction defect in DSCFT simulations. Data are plotted according to the same criteria as in Figure 9b. Selected frames from the simulation movie show characteristic (A and B) and intermediate stages of the 3T-junction movement. Solid arrows (red) mark the left edge of the 3T-junction upon propagation.

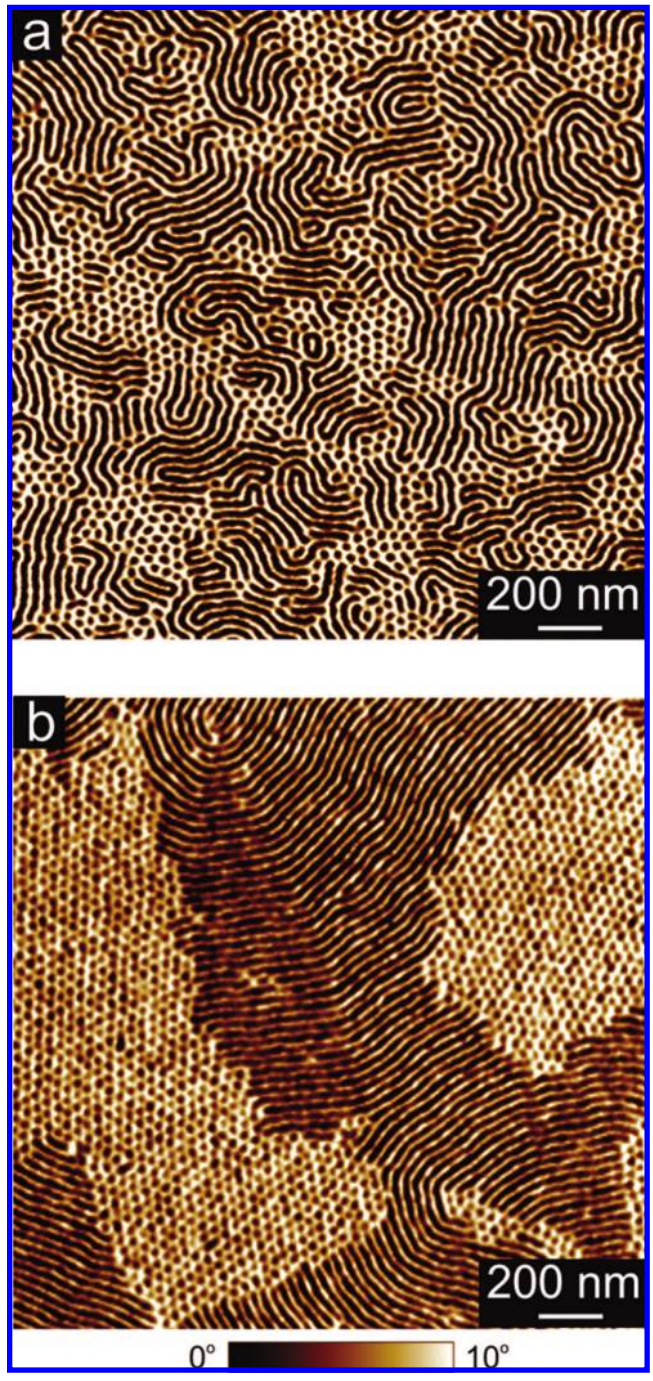

Figure 11. SFM phase images presenting coexisting PL and cylinder morphologies in SB films annealed for 18 hours (a) in vacuum at 120 °C on carbon coated silicon and (b) on silicon substrate under the atmosphere of 50% of the saturated chloroform vapor pressure.

equilibration is higher under solvent annealing conditions. Further comparison of images in Figure 11a,b suggests that both the density of defects and their relative lifetimes depend on the chain mobility. In thermally annealed films, all types of described above classic and modified defects (Figures 36 and 8) appear to be kinetically trapped. In swollen films, specific neck defects obviously dominate over other defect types which presumably have short life-times under these conditions (Figures 7e,f and 11b).

We believe that in thermally annealed films, the lateral coarsening of the PL grains proceeds predominantly through the lateral movement of PL-modified or clustered complex defect configurations such as PL-patches and T-junctions (Figures 8–10). In solvent-containing systems with considerable interfacial fluctuations, the neck-defects are involved in the grain coarsening at late stages of structure equilibration. It is likely that motion of neck defects, doubled necks (which are structurally similar to a single PL ring) along the cylinder axis, and their interaction with other defects or with existing grains of nonbulk phases can be considered as elementary steps of the lateral separation of morphologies in thermal coexistence (Figures 7f and 11b).

SUMMARY

In this work, we focus on specific defects in the cylinder phase which are kinetically trapped in thermal equilibrium during the lateral ordering of lying microdomains. Using SFM measurements complemented by DSCFT simulations we show that structural defects and their interactions in cylinder-forming block copolymers can not always be described with the approaches and knowledge gained from defect studies in nematic thermotropic and lyotropic liquid crystals. In particular, the systems studied here showed a strong correlation between the defect structure and chain mobility both on short and on long-term time scales.

We have shown that purely topological arguments and 2D representation are not sufficient to elucidate the stability and mobility of defects in cylinder morphology where specific and representative classic defects provide connectivity of cylinders (of the minority component). Generally, dislocations with a closed cylinder end are more stable than configurations with an open cylinder end which are typically short-lived elementary steps of defect reconstruction. Classical +1/2 disclinations in the cylinder phase incorporate alternative structures, such as the nonbulk perforated lamella phase which has planar symmetry and thus a higher degree of connectivity of the minority component. Observation of nonsingular neck defects suggests similarities of transport mechanisms in block copolymers with considerable interfacial fluctuations and in other types of soft matter such as lyotropic liquid crystals and membranes.

Good agreement between the experiment and simulations on the details of the lateral propagation of a complex 3T-junction defect suggests diffusion-driven

lateral transport and correlated defect motion due to the interconnectivity of the polymer chains. Additionally, simulation results show that the bottom (wetting) layer is only weakly involved in the development of the structures at the free surface. The estimates of the motion velocity of the clustered defect configurations give insight into the molecular mechanisms of the chain transport in block copolymer materials.

The degree of lateral separation of coexisting PL and cylinder phases and related representative defects depend on the mobility of chains under given annealing conditions. Our results suggest that the chain mobility is an important factor that guides the pathways of defect annihilation and thus the transport mechanisms in block copolymer films.

EXPERIMENTAL DETAILS

Polymer. We used polystyrene-*block*-polybutadiene copolymer (SB) (Polymer Source Inc.) with molecular weights of the polystyrene (PS) and polybutadiene (PB) blocks of 13.6 and 33.7 kg/mol, respectively, with a PS volume fraction of 25.5% and a polydispersity of 1.02. The glass transition temperatures of the SB components are $T_{g,PB} = -60$ °C and $T_{g,PS} = 80-100$ °C. In bulk, SB forms glassy PS cylinders embedded in a soft PB matrix with a characteristic distance of 33.6 nm between the next-nearest cylinders (SAXS measurements).[34] SB films were prepared by spincoating a toluene solution on carbon-coated silicon wafers and further annealing either under chloroform (nearly neutral solvent) at controlled vapor pressure or at elevated temperatures in vacuum.

Scanning Force Microscopy. The microdomain morphology in quenched films was measured with a Dimension 3100 SFM (Veeco Instruments Inc.) operated in TappingMode using silicon tips with a spring constant of *ca.* 40 N/m, and a resonance frequency ranging from 200 to 300 kHz.

In-situ imaging was performed in the hot-stage of a MultiMode SFM (DI/Veeco Metrology Group) under a flow of dry nitrogen, with an amplitude setpoint of ~0.96 and a scanning frequency of 9 Hz, resulting in an acquisition time of 46 s/image. An 50 nm thick SB film on carbon coating was first annealed at 140 °C to induce terrace formation and lateral ordering of the microdomains and then quenched to 105 °C for SFM imaging. At the temperature range 105−120 °C, the combined Flory-Huggins parameter χN is about 35, which corresponds to the intermediate segregation regime.

To estimate the possible impact of the sample degradation due to the loose seal of the heating chamber, we performed separate snapshot measurements under the above temperature and nitrogen flow conditions. The first signs of the partial cross-linking of the PB component were detected after 20 hours of annealing, which considerably exceeds the typical times of the *in-situ* measurements.

Simulation. Thin film behavior of a cylinder-forming block copolymer was modeled using the dynamic variant of self consistent field theory (DSCFT).[48] Earlier this method was successfully used to study equilibrium structures,[31,32,49] dynamics of phase transitions,[38] and structure evolution in supported films.[43] Since the governing equation for structure evolution in DSCFT is a stochastic differential equation, where the stochastic term represents the thermal fluctuations, the morphology of thin film as well as the appearance and connectivity of structural defects is not predefined.

For the analysis of defects in one-layer-thick films of cylinder-forming block copolymers, we have considered three systems which phase behavior has been described in detail in earlier publications.[32,49] Systems A and B from ref 32 both have symmetric wetting conditions, with a film height of 7 grid units (+2 grid units for the mask) and the interaction parameter between the polymer beads $\varepsilon_{AB} = 6.5$. The interaction parameters of the polymer beads with the surfaces (or with the mask) are $\varepsilon_{AS} = 5$, $\varepsilon_{BS} = 0$, and $\varepsilon_{AS} = 6$; $\varepsilon_{BS} = 0$ for systems A and B, respectively. System C from ref 49 has asymmetric wetting conditions, a film height of 10 grid units (+2 grid units for mask); $\varepsilon_{AB} = 6.5$, and the interaction parameters of the polymer beads with the lower interface $\varepsilon_{AS} = 6$, $\varepsilon_{BS} = 0$, and with the upper interface $\varepsilon_{AS1} = -1$, $\varepsilon_{BS1} = 0$. For the present study the above systems have been simulated in large boxes with lateral sizes of 128 × 128 grids to exclude the influence of the boundary conditions on single defects; the examples of classical and specific defects in Figures 3–6, 8 are cuts (in time and position) from these simulations. For each system simulations have been done for more than 50000 simulation steps. We note that the simulation results cannot be used for the independent statistical analysis of the representative defect configurations as even the largest simulation boxes contain not more than 20 microdomains. Here simulations are used to support experimental observations, which give access to a statistically valuable number of defect configurations.

The dynamics of a complex 3T-junction defect was followed in system C in the simulation box with lateral sizes of 64 × 64 grid units (Figure 10).

Acknowledgment. This work was supported by the Sonderforschungsbereich 481 (TP B7, A8) funded by the Deutsche Forschungsgemeinschaft (D.F.G.). G. Krausch and R. Magerle are gratefully acknowledged for fruitful discussions.

Supporting Information Available: SFM movie: Tapping-mode scanning force microscopy movie of the surface structures in a fluid SB film at 105 °C. Bright color corresponds to PS microdomains. The size of the area is 350 × 350 nm^2. The frame rate is 46 s/frame, and the total imaging time is ~92 min. Simulational movie: Dynamic self-consistent mean-field simulations of the structure evolution in cylinder-forming block copolymer melt modeled by A3B12A3 Gaussian chains. The dimensions of the simulation box are 64 × 64 × 12 grid units. The displayed A-component (isodensity level $\rho_A = 0.5$) forms one structured layer on the top of wetting layer. The surface fields are set to $\varepsilon_{M,1} = -1$ kJ/mol and $\varepsilon_{M,2} = 5$ kJ/mol. The structure dynamics is plotted every 50th time step in the simulation range from 3000 to 10000 time steps. This material is available free of charge *via* the Internet at http://pubs.acs.org.

REFERENCES AND NOTES

1. Fasolka, M. J.; Mayes, A. M. Block Copolymer Thin Films: Physics and Applications. *Annu. Rev. Mater. Res.* **2001**, *31*, 323–355.
2. Segalman, R. A. Patterning with Block Copolymer Thin Films. *Mater. Sci. Eng. Res.* **2005**, *R48*, 191–226.
3. Darling, S. B. Directing the Self-Assembly of Block Copolymers. *Prog. Polym. Sci.* **2007**, *32*, 1152–1204.
4. Stein, G. E.; Cochran, E. W.; Katsov, K.; Fredrickson, G. H.; Kramer, E. J.; Li, X.; Wang, J. Symmetry Breaking of in-Plane Order in Confined Copolymer Mesophases. *Phys. Rev. Lett.* **2007**, *98*, 158302–158304.
5. Kim, S. O.; Kim, B. H.; Kim, K.; Koo, C. M.; Stoykovich, M. P.; Nealey, P. F.; Solak, H. H. Defect Structure in Thin Films of a Lamellar Block Copolymer Self-Assembled on Neutral Homogeneous and Chemically Nanopatterned Surfaces. *Macromolecules.* **2006**, *39*, 5466–5470.
6. Sundrani, D.; Darling, S. B.; Sibener, S. J. Guiding Polymers to Perfection: Macroscopic Alignment of Nanoscale Domains. *Nano Lett.* **2004**, *4*, 273–276.
7. Edwards, E. W.; Montague, M. F.; Solak, H. H.; Hawker, C. J.; Nealey, P. F. Precise Control over Molecular Dimensions of Block-Copolymer Domains Using the Interfacial Energy of Chemically Nanopatterned Substrates. *Adv. Mater.* **2004**, *16*, 1315–1319.
8. Corte, L.; Yamauchi, K.; Court, F.; Cloitre, M.; Hashimoto, T.; Leibler, L. Annealing and Defect Trapping in Lamellar Phases of Triblock Terpolymers. *Macromolecules.* **2003**, *36*, 7695–7706.
9. Huang, E.; Mansky, P.; Russell, T. P.; Harrison, C.; Chaikin, P. M.; Register, R. A.; Hawker, C. J.; Mays, J. Mixed Lamellar Films: Evolution, Commensurability Effects, and Preferential Defect Formation. *Macromolecules* **2000**, *33*, 80–88.

10. Amundson, K.; Helfand, E.; Quan, X.; Hudson, S. D.; Smith, S. D. Alignment of Lamellar Block Copolymer Microstructure in an Electric Field. 2. Mechanisms of Alignment. *Macromolecules* **1994**, *27*, 6559–6570.
11. Cohen, Y.; Thomas, E. L. Effect of Defects on the Response of a Layered Block Copolymer to Perpendicular Deformation: One-Dimensional Necking. *Macromolecules* **2003**, *36*, 5265–5270.
12. Fredrickson, G. H.; Ganesan, V.; Drolet, F. Field-Theoretic Computer Simulation Methods for Polymers and Complex Fluids. *Macromolecules* **2002**, *35*, 16–39.
13. Bosse, A. W.; Sides, S. W.; Katsov, K.; Garcia-Cervera, C. J.; Fredrickson, G. H. Defects and Their Removal in Block Copolymer Thin Film Simulations. *J. Polym. Sci., Part B: Polym. Phys.* **2006**, *44*, 2495–2511.
14. Netz, R. R.; Andelman, D.; Schick, M. Interfaces of Modulated Phases. *Phys. Rev. Lett.* **1997**, *79*, 1058–1061.
15. Tsori, Y.; Andelman, D.; Schick, M. Defects in Lamellar Diblock Copolymers: Chevron- and W-Shaped Tilt Boundaries. *Phys. Rev. E* **2000**, *61*, 2848–2858.
16. Zvelindovsky, A. V.; Sevink, G. J. A. Comment on "Microscopic Mechanisms of Electric-Field-Induced Alignment of Block Copolymer Microdomains". *Phys. Rev. Lett.* **2003**, *90*, 049601.
17. Harrison, C.; Adamson, D. H.; Cheng, Z.; Sebastian, J. M.; Sethuraman, S.; Huse, D. A.; Register, R. A.; Chaikin, P. M. Mechanisms of Ordering in Striped Patterns of Diblock Copolymers. *Science* **2000**, *290*, 1558–1561.
18. Hahm, J.; Lopes, W. A.; Jaeger, H. M.; Sibener, S. J. Defect Evolution in Ultrathin Films of Polystyrene-*block*-poly(methyl methacrylate) Diblock Copolymers Observed by Atomic Force Microscopy. *J. Chem. Phys.* **1998**, *109*, 10111–10114.
19. Hahm, J.; Sibener, S. J. Time-Resolved Atomic Force Microscopy Imaging Studies of Asymmetric PS-B-PMMA Ultrathin Films: Dislocation and Disclination Transformations, Defect Mobility, and Evolution of Nanoscale Morphology. *J. Chem. Phys.* **2001**, *114*, 4730–4740.
20. Hammond, M. R.; Cochran, E.; Fredrickson, G. H.; Kramer, E. J. Temperature Dependence of Order, Disorder, and Defects in Laterally Confined Diblock Copolymer Cylinder Monolayers. *Macromolecules* **2005**, *38*, 6575–6585.
21. Segalman, R. A.; Hexemer, A.; Hayward, R. C.; Kramer, E. J. Ordering and Melting of Block Copolymer Spherical Domains in 2 and 3 Dimensions. *Macromolecules* **2003**, *36*, 3272–3288.
22. Rider, D. A.; Cavicchi, K. A.; Vanderark, L.; Russell, T. P.; Manners, I. Orientationally Controlled Nanoporous Cylindrical Domains in polystyrene-*b*-poly(ferrocenylethylmethylsilane) Block Copolymer Films. *Macromolecules.* **2007**, *40*, 3790–3796.
23. Harrison, C.; Adamson, D. H.; Trawick, M.; Angelescu, D. E.; Cheng, Z.; Huse, D. A.; Chaikin, P. M.; Vega, D. A.; Sebastian, J. M.; Register, R. A. Pattern Coarsening in a 2D Hexagonal System. *Europhys. Lett.* **2004**, *67*, 800–806.
24. Cheng, J. Y.; Mayes, A. M.; Ross, C. A. Nanostructure Engineering by Templated Self-Assembly of Block Copolymers. *Nat. Mater.* **2004**, *3*, 823–828.
25. Hammond, M. R.; Sides, S. W.; Fredrickson, G. H.; Kramer, E. J.; Ruokolainen, J.; Hahn, S. F. Adjustment of Block Copolymer Nanodomain Sizes at Lattice Defect Sites. *Macromolecules* **2003**, *36*, 8712–8716.
26. Mueller, M.; Katsov, K.; Schick, M. A New Mechanism of Model Membrane Fusion Determined from Monte Carlo Simulation. *Biophys. J.* **2003**, *85*, 1611–1623.
27. Katsov, K.; Müller, M.; Schick, M. Field Theoretic Study of Bilayer Membrane Fusion: II. Mechanism of a Stalk-Hole Complex. *Biophys. J.* **2006**, *90*, 915–926.
28. Constantin, D.; Oswald, P. Diffusion Coefficients in a Lamellar Lyothropic Phase: Evidence for Defects Connecting the Surfactant Structures. *Phys. Rev. Lett.* **2000**, *85*, 4297.
29. Matsen, M. W. Elastic Properties of a Diblock Copolymer Monolayer and Their Relevance to Bicontinuous Microemulsion. *J. Chem. Phys.* **1999**, *110*, 4658–4667.
30. Matsen, M. W.; Schick, M. Stable and Unstable Phases of a Linear Multiblock Copolymer Melt. *Macromolecules* **1994**, *27*, 7157–7163.
31. Knoll, A.; Horvat, A.; Lyakhova, K. S.; Krausch, G.; Sevink, G. J. A.; Zvelindovsky, A. V.; Magerle, R. Phase Behavior in Thin Films of Cylinder-Forming Block Copolymers. *Phys. Rev. Lett.* **2002**, *89*, 035501–035501/035504.
32. Horvat, A.; Lyakhova, K. S.; Sevink, G. J. A.; Zvelindovsky, A. V.; Magerle, R. Phase Behavior in Thin Films of Cylinder-Forming ABA Block Copolymers: Meso Scale Modeling. *J. Chem. Phys.* **2004**, *120*, 1117–1126.
33. Huinink, H. P.; van Dijk, M. A.; Brokken-Zijp, J. C. M.; Sevink, G. J. A. Surface-Induced Transitions in Thin Films of Asymmetric Diblock Copolymers. *Macromolecules.* **2001**, *34*, 5325–5330.
34. Tsarkova, L.; Knoll, A.; Krausch, G.; Magerle, R. Substrate-Induced Phase Transitions in Thin Films of Cylinder-Forming Diblock Copolymer Melts. *Macromolecules.* **2006**, *39*, 3608–3615.
35. de Gennes, P. G.; Prost, J. *The Physics of Liquid Crystals*; Clarendon Press: Oxford, U.K., 1993.
36. Chaikin, P. M.; Lubensky, T. C. *Principles of Condenced Matter Physics*; Cambridge University Press: New York, 1995; Chapter 9.
37. Tsarkova, L.; Knoll, A.; Magerle, R. Rapid Transitions between Defect Configurations in a Block Copolymer Melt. *Nano Lett.* **2006**, *6*, 1574–1577.
38. Knoll, A.; Horvat, A.; Lyakhova, K. S.; Krausch, G.; Sevink, G. J. A.; Zvelindovsky, A. V.; Magerle, R. Direct Imaging and Mesoscale Modelling of Phase Transitions in a Nanostructured Fluid. *Nat. Mater.* **2004**, *3*, 886–891.
39. Tsarkova, L.; Horvat, A.; Krausch, G.; Zvelindovsky, A. V.; Sevink, G. J. A.; Magerle, R. Defect Evolution in Block Copolymer Thin Films *via* Temporal Phase Transitions. *Langmuir* **2006**, *22*, 8089–8095.
40. Duque, D.; Schick, M. Self-Consistent Field Theory of Twist Grain Boundaries in Block Copolymers. *J. Chem. Phys.* **2000**, *113*, 5525–5530.
41. SFM movie, see Supporting Information.
42. Simulation movie, see Supporting Information.
43. Horvat, A.; Knoll, A.; Krausch, G.; Tsarkova, L.; Lyakhova, K. S.; Sevink, G. J. A.; Zvelindovsky, A. V.; Magerle, R. Time Evolution of Surface Relief Structures in Thin Block Copolymer Films. *Macromolecules.* **2007**, *40*, 6930–6939.
44. Kim, H.-C.; Russell, T. P. Ordering in Thin Films of Asymmetric Diblock Copolymers. *J. Polym. Sci., Part B* **2001**, *39*, 663–668.
45. Lin, Y.; Böker, A.; Sill, K.; Xiang, H.; Abetz, C.; Wang, J.; Emrick, T.; Balazs, A.; Russell, T. P. Self-Directed Self-Assembly of Nanoparticle/Copolymer Mixtures. *Nature.* **2005**, *434*, 55–59.
46. Kim, S. H.; Misner, M. J.; Russell, T. P. Solvent-Induced Ordering in Thin Film Diblock Copolymer/Homopolymer Mixtures. *Adv. Mater.* **2004**, *16*, 2119–2123.
47. Tsarkova, L. In *Nanostructured Soft Matter:Experiment, Theory, Simulation and Perspectives.* Zvelindovsky, A. V., Ed.; Springer: Heidelberg, Germany, 2007; 231–266.
48. Sevink, G. J. A.; Zvelindovsky, A. V.; van Vlimmeren, B. A. C.; Maurits, N. M.; Fraaije, J. Dynamics of Surface Directed Mesophase Formation in Block Copolymer Melts. *J. Chem. Phys.* **1999**, *110*, 2250–2256.
49. Lyakhova, K. S.; Sevink, G. J. A.; Zvelindovsky, A. V.; Horvat, A.; Magerle, R. Role of Dissimilar Interfaces in Thin Films of Cylinder-Forming Block Copolymers. *J. Chem. Phys.* **2004**, *120*, 1127–1137.